Short-range interaction in liquid rhodium probed by x-ray absorption spectroscopy

1999 J. Phys.: Condens. Matter 11 L43

(http://iopscience.iop.org/0953-8984/11/6/001)

J. Phys.: Condens. Matter **11** (1999) L43–L49. Printed in the UK PII: S0953-8984(99)98696-4

LETTER TO THE EDITOR

Short-range interaction in liquid rhodium probed by x-ray absorption spectroscopy

Andrea Di Cicco†, Giuliana Aquilanti†, Marco Minicucci†, Adriano Filipponi‡ and Jaroslaw Rybicki§

† UdR INFM, Dipartimento di Matematica e Fisica, Università degli Studi di Camerino Via Madonna delle Carceri, 62032 Camerino (MC), Italy

‡ UdR INFM, Dipartimento di Fisica, Università dell' Aquila, 67010 Coppito, L'Aquila, Italy

§ Technical University of Gdansk, Naturowicza 11/12, 80-952 Gdansk, Poland

Received 23 October 1998

Abstract. Accurate XAFS spectra of solid and liquid rhodium at very high temperature have been recorded at the European Synchrotron Radiation Facility. Experiments have been analysed using advanced data analysis techniques and the results are compared with molecular dynamics simulations performed using several different pair functionals as model potentials. High-temperature data provided new insight on the details of the interaction potential allowing us to test the validity of different functional forms. The short-range $g(r)$ at about 2300 K of liquid Rh and of the Rh–C alloy near the eutectic composition are measured for the first time and compared with MD results.

The availability of high-brilliance third generation synchrotron radiation sources has opened new opportunities for the study of condensed matter under extreme conditions at high pressure and/or high temperature. The x-ray absorption spectroscopy (XAS) has been exploited up to the 100 GPa high-pressure range [1]. Temperatures up to about 2000 K and pressures of about 2 kbar can be reached using sapphire cells in an autoclave system [2], a technique exploited for the study of fluid Se up to the critical point [2, 3]. XAS measurements up to about 1500 K and 50 kbar can be performed using a technique based on the use of the Paris–Edinburgh press [4] and recent experiments on fluid I_2 have been performed [5]. A containerless technique based on electromagnetic levitation of molten and highly undercooled liquid specimens has been also developed for high-temperature XAS experiments [6].

An alternative technique for high-temperature low-noise XAS experiments in high-vacuum conditions is based on the measurement of sintered pellets of fine sample particles and an inert matrix powder [7]. It has been exploited for the study of liquid and undercooled liquid metals like Ge [8] and Sn [9] and was recently made available at the BM29 x-ray absorption spectrometer of the European Synchrotron Radiation Facility (ESRF) [10].

Recent advances in the data analysis of the x-ray absorption fine structure (XAFS) [11] have opened the way for the establishment of a reliable methodology for investigating highly disordered systems. XAFS is particularly sensitive to the shape of the first peak of the pair distribution function and can complement information on the medium- and long-range order obtained, for instance, from diffraction techniques [8, 9, 12]. The possibility of testing the short-range part of the interatomic potential by comparing XAS results to the model structure provided by Monte Carlo (MC) or molecular dynamics (MD) computer simulations has been emphasized [13].

0953-8984/99/060043+07$19.50

In this letter we report the results of a challenging experimental achievement such as the first XAS measurement of liquid rhodium (melting point $T_m \sim 2236$ K), which has been performed at the third generation ESRF BM29 spectrometer. Due to the high T_m no diffraction measurements have so far been reported for this system. The XAFS data of solid and liquid Rh are analysed using calculations of the x-ray absorption cross-section in the framework of the GNXAS method [11]. Results on high-temperature solid and liquid Rh are compared with structural models obtained using MD simulations performed using different pair functionals [14, 15] developed in recent years for transition metals.

The Rh K-edge XAS measurements were performed using a Si(311) double crystal monochromator. The primary vertical slit were set to 0.5 mm achieving a typical resolution of about 1.5 eV at 30 keV. XAS spectra were measured in transmission mode using ionization chambers. High-temperature XAFS measurements were performed under high vacuum condition $\approx 10^{-5}$ mbar using an improved version of the previously described oven [7, 10]. The sample temperature was measured using an optical pyrometer in the 1000–2500 K range and various sets of thermocouples up to about 1800 K.

Samples suitable for high-temperature studies were produced by mixing ammonium hexachlororhodate fine powder (99.999% purity) with different matrices such as high-purity graphite, BN, ZrO_2 and HfO_2. The Rh salt was decomposed and reduced by an *in situ* heat treatment into micrometric size metallic grains embedded in the matrix powder. Crucible materials such as graphite 100 μm thick for the Rh/C sample, Mo 2.5 μm, Ta 2 μm, and W 5 μm for the other matrices, were used.

Good quality measurements of solid Rh in the 300–1900 K temperature range were obtained in a wide wave-vector range (up to $k \sim 25$ Å^{-1}) using both Rh/C pellets and a 25 μm Rh foil heated directly through the electrodes. In the case of the Rh/C sample the reversible diffusion of C in Rh is observed above 1600 K, in agreement with the known Rh–C phase diagram [16], leading to the melting of a Rh–C alloy with the eutectic composition. Attempts to measure pure liquid Rh using BN or ZrO_2 matrices were not successful due to the occurrence of chemical reactions. Successful measurements of pure liquid Rh just above the melting point were instead possible using the HfO_2 matrix and a W crucible. The difficulty of collecting good quality spectra was enhanced by the high absorption of the crucible and of the matrix, by the small sample size (about 1 mm^2) and relatively short lifetime of the crucible at very high temperature. For this reason the high photon flux provided by ESRF was essential to obtain low-noise XAS spectra. Raw XAS data of liquid Rh and liquid Rh–C alloy around the eutectic composition are shown in figure 1.

Realistic structural models for solid and liquid Rh were obtained by classical MD calculations, performed using 864 atoms and experimental density values for temperatures ranging from 100 to 3000 K. We used previously published pair functionals for which the attractive part is computed using the second-moment approximation within the tight-binding scheme. Two different functional forms containing a square-root (1/2Ros) [14] or a 2/3 dependence from the effective coordination were used. Two different 2/3 models has been proposed in [15]. The first, hereafter referred as 2/3Gue-f1, has been derived using as experimental constraints the cohesive energy, the bulk modulus and the elastic constant (C_{44}), while the second (2/3Gue-f2) has been calculated by introducing the vacancy formation energy instead of C_{44}.

First-neighbour average distances R and bond variances σ^2 obtained from MD simulations of solid Rh are compared with XAFS experimental results in figure 2 (data with error bars). Note that XAFS (and MD) measure the interatomic distances including the contribution of vibrations perpendicular to the bond direction (see [8] and references therein). Therefore, the slight elongation of the average distance with respect to the cell parameter $a = \sqrt{2}R$ measured

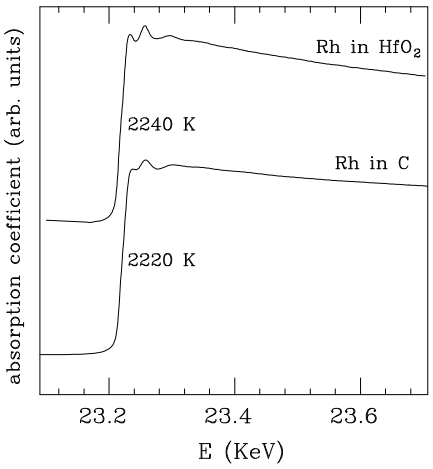

Figure 1. Raw x-ray absorption data of liquid Rh dispersed into HfO_2 (upper curve) and graphite (lower curve).

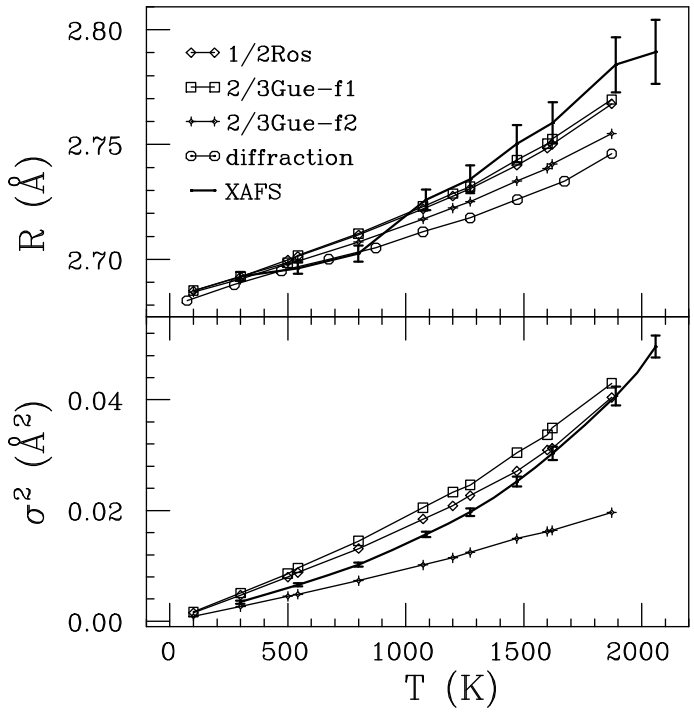

Figure 2. First-shell distance R and variance σ^2 of solid Rh as a function of temperature obtained from XAFS data analysis (data with error bars) compared with those determined from MD simulations and with the mean equilibrium site-to-site distance measured by diffraction.

by diffraction [16], obtained increasing the temperature, is a normal effect. The first-neighbour variance at high temperature is in quite good agreement with MD results using 1/2Ros and 2/3Gue-f1 models while is not compatible with that predicted using the 2/3Gue-f2 potential.

At moderate temperatures, 300–1000 K, the experimental bond variance lies in between the 1/2Ros and 2/3Gue-f2 curves. The inaccuracy of the 2/3 Gue-f2 potential in describing the local structure of high-temperature Rh was also verified looking at the third cumulants of the distribution (not shown) and melting point which was found to lie at much higher temperature than the known experimental value.

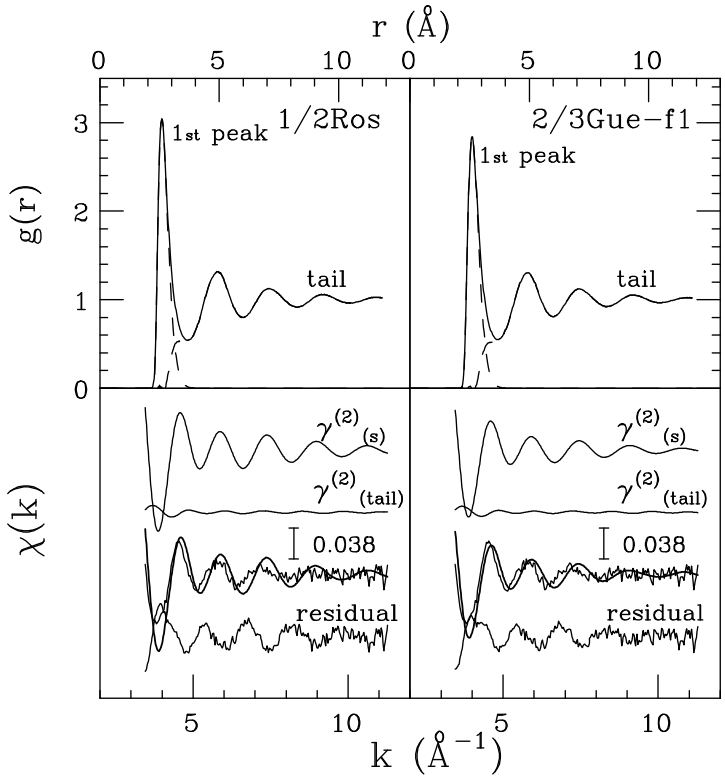

Figure 3. Upper panels: $g(r)$ of liquid Rh at about 2500 K obtained from MD simulations decomposed into first-neighbour peaks and long-range tails. Lower panels: model $\gamma^{(2)}$ signals calculated from corresponding $g(r)$ functions (upper panels) compared with $\chi(k)$ XAFS experimental data.

XAS data of liquid systems can be analysed starting from a model $g(r)$ which satisfies the correct long-range conditions [17]. Realistic model $g(r)$ functions are provided by MD simulations of liquid Rh at 2500 K using the above mentioned 1/2Ros and 2/3Gue-f1 pair functionals (see figure 3, upper panels). The $g(r)$ functions were decomposed into short-range peaks and long-range tails (dashed curves in figure 3). XAS data analysis can provide a refinement only of the short-range $g(r)$ peak, parametrized using the mean distance, variance and asymmetry parameters [17]. Model $\gamma^{(2)}$ two-body signals [11] related to the short-range peaks and to the tail of the corresponding $g(r)$ (upper panels) are compared with experimental XAFS $\chi(k)$ data in the lower panels of figure 3. The main contribution $\gamma^{(2)}_{(S)}$ to the experimental signal is clearly associated with the short-range peak. Both calculations are in qualitative agreement with experimental data. However, the evident oscillation in the residual curve (bottom in figure 3) indicates that a refinement of the short-range part of the $g(r)$ is necessary.

Best-fit $\gamma^{(2)}_{(S)}$ and the (fixed) tail signal $\gamma^{(2)}_{(tail)}$ are reported in figure 4, upper panel. The

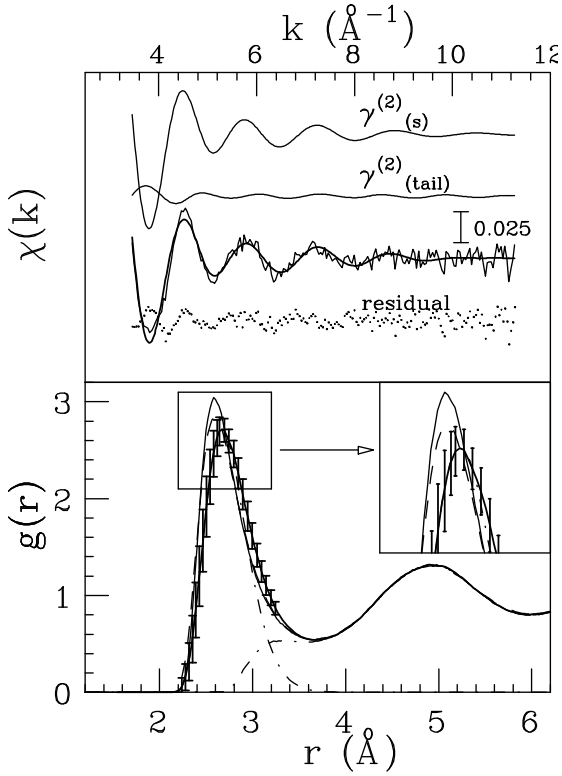

Figure 4. Upper panel: best-fit calculated signals associated with the short range part ($\gamma^{(2)}_{(S)}$) and the tail of the liquid Rh $g(r)$ at 2240 K. The total best-fit curve is compared with $\chi(k)$ experimental data. Lower panel: comparison between the $g(r)$ reconstructed by XAFS (thick solid curve with error bars) and those obtained by MD simulations (solid and dashed curves). A magnification of the peak is drawn in the inset.

result of the fit, obtained by summing the individual contributions, is compared with liquid Rh experimental data at 2240 K (solid curves, bottom). The agreement is excellent as shown by the residual curve (dots). The reconstructed $g(r)$ (thick solid) and its decomposition into the best-fit short-range peak and tail functions (dot-dashed) are shown in figure 4, lower panel. Error bars were evaluated for a 95% confidence level and accounting for correlations among the relevant parameters. The best-fit $g(r)$ is compared with the initial MD models (solid and dashed curves). For liquid Rh the best-fit curve results are in better agreement with the 2/3 Gue-f1 model. A portion of the figure is magnified in the inset where the shift toward longer distances ($\sim$0.1 Å) of the first peak, with respect to both MD results, is evidenced. The foot of the distribution remains approximately at the same distance and the rise of the $g(r)$ is less steep than that calculated by MD. This is an indication that a softer interatomic potential would better reproduce the local structure of liquid Rh.

Using the present XAS high-temperature technique it was also possible to measure a Rh–C alloy with a concentration close to the eutectic composition. In this case, very low-noise measurements are possible due to the very low absorption of the matrix and crucible. The Rh–C system melts at about 1967 K with a carbon atomic fraction of about 16% (eutectic composition) [16] and the shape of XAS data is clearly different from that of pure liquid Rh as shown in figure 1. The experimental XAFS $\chi(k)$ signal measured at about 2220 K

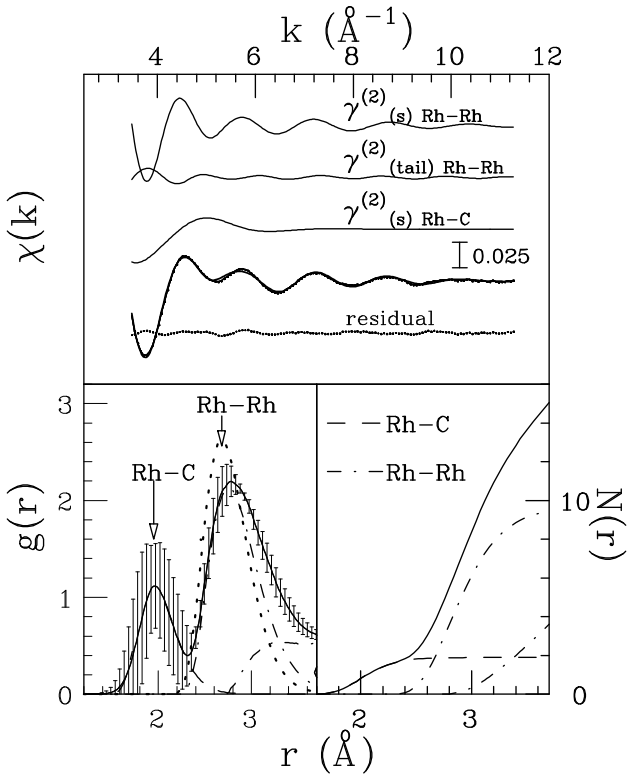

Figure 5. Upper panel: Comparison of experimental and calculated best-fit $\chi(k)$ XAFS signals related to liquid Rh–C alloy at 2220 K. The agreement is very good, as shown by the residual curve (bottom). Individual Rh–Rh and Rh–C contributions are reported (top). Left-lower panel: reconstructed $g(r)$ associated with Rh–Rh and Rh–C signals (data with error bars). The $g(r)$ is decomposed into its short- and long-range components (dot-dashed) and compared with the first $g(r)$ peak of pure liquid Rh reported in figure 4 (large dots). Right-lower panel: coordination numbers $N(r)$ associated with C (dashed) and Rh (dot-dashed) atoms as a function of distance from a generic Rh atom. The total $N(r)$ is also shown (solid).

is compared in figure 5 with the best-fit calculated curve obtained taking into account the presence of C atoms at short distances (upper panel). Inclusion of a Rh–C $\gamma^{(2)}$ signal was found to be necessary to explain the experimental data. Thus, the model signal included Rh–Rh and Rh–C $\gamma^{(2)}_{(S)}$ short-range terms while long-range contributions were approximated using the 1/2Ros Rh–Rh tail neglecting possible, although certainly very weak, Rh–C contributions. The individual best-fit Rh–Rh and Rh–C $\gamma^{(2)}_{(S)}$ terms are shown in the same frame of figure 5 (top). The best-fit was performed floating both the Rh–Rh and Rh–C mean distance, variance and asymmetry parameters. The Rh–C coordination number was also floated. The agreement between calculated and experimental XAFS is very good, as shown by the residual curve in figure 5.

The final best-fit parameter values allowed us to reconstruct the $g(r)$ centred on Rh atoms shown in figure 5, left-lower panel. An evident peak due to C atoms at very short distances is found, with mean distance $R \sim 2.06$ Å, compatible with typical metal-C bond-lengths. The final best-fit Rh–C coordination number $N \sim 1.9$ (dashed, right-lower panel) is compatible with a C dilution in the range 15–20%, near the eutectic composition. Presence of C atoms

at short distances causes a shift of the Rh–Rh first-neighbour peak toward longer distances ($\sim$ 0.1 Å). The peak is also slightly broadened compared with pure liquid Rh (dots). The running Rh–C and Rh–Rh coordination numbers as functions of distance $N(r)$ are reported in the right-lower panel of figure 5. The total $N(r)$ (solid) increases to typical close-packed values reaching 12 atoms at about 3.3 Å.

Results reported in the present letter show that reliable very high-temperature XAS measurements of liquid metals and alloys are feasible using third generation synchrotron radiation sources and available experimental devices. Experimental XAS results for high-temperature Rh have been compared with structural models obtained using MD simulations allowing us to evaluate the accuracy of different proposed microscopic interaction potentials in transition elements. The short-range part of the pair distribution function of liquid Rh at 2240 K was measured for the first time showing that the first peak is slightly broadened and shifted toward longer distances compared with MD simulations. The short-range structure of the Rh–C alloy at about 2220 K near the eutectic composition was also determined. An evident peak in the $g(r)$ associated with the presence of C atoms around 2 Å and a clear elongation of the average Rh–Rh distance were found. These findings should stimulate further experimental efforts to study local structure and interatomic interactions in liquid metals and alloys in extreme conditions.

References

[1] Itiè J P, Polian A, Martinez D, Briois V, Di Cicco A, Filipponi A and San Miguel A 1997 *J. Physique (Paris)* **7** C2–31

[2] Hosokawa S, Tamura K, Inui M, Yao M, Endo H, and Hoshino H 1992 *J. Chem. Phys.* **97** 786
Tamura K, Inui M and Hosokawa S 1995 *Rev. Sci. Instrum.* **66** 1382

[3] Soldo Y, Hazemann J L, Aberdam D, Inui M, Tamura K, Raoux D, Pernot E, Jal J F and Dupuy-Philon J 1998 *Phys. Rev.* B **57** 258

[4] Katayama Y, Mezouar M, Itiè J P, Besson J M, Syfosse G, Le Fevre P and Di Cicco A 1997 *J. Physique (Paris)* **7** C2–1011

[5] Buontempo U, Filipponi A, Martinez-Garcia D, Postorino P, Mezouar M and Itiè J P 1998 *Phys. Rev. Lett.* **80** 1912

[6] Jacobs G, Egry I, Maier K, Platzek D, Reske J and Frahm R 1996 *Rev. Sci. Instrum.* **67** 3683

[7] Filipponi A and Di A Cicco 1994 *Nucl. Instrum. Methods Phys. Res.* B **93** 302

[8] Filipponi A and Di A Cicco 1995 *Phys. Rev.* B **51** 12322

[9] Di Cicco A and Filipponi A 1996 *J. Non-Cryst. Solids* **205–207** 304

[10] Filipponi A, Borowski M, Loeffen P W, De Panfilis S, Di Cicco A, Sperandini F, Minicucci M and Giorgetti M 1998 *J. Phys.: Condens. Matter* **10** 235

[11] Filipponi A, Di Cicco A and Natoli C R 1995 *Phys. Rev.* B **52** 15122

[12] Di Cicco A, Minicucci M and Filipponi A 1997 *Phys. Rev. Lett.* **78** 460

[13] Di Cicco A, Filipponi A, Itiè J P and Polian A 1996 *Phys. Rev.* B **54** 9086

[14] Cleri F and Rosato V 1993 *Phys. Rev.* B **48** 22

[15] Guevara J, Llois A M and Weissmann M 1995 *Phys. Rev.* B **52** 11509

[16] Madelung O (ed) 1992 *Numerical Data and Functional Relationships in Science and Technology (Landolt-Börnstein Series)* vol IV/5 (Berlin: Springer)
Hellwege K-H and Hellwege A M (eds) 1988 *Numerical Data and Functional Relationships in Science and Technology (Landolt-Börnstein Series)* vol III/14 (Berlin: Springer)

[17] Filipponi A 1994 *J. Phys.: Condens. Matter* **6** 8415